

Article

The Use of a Saturated Long Carbon Chain Sodium Monocarboxylate for the Corrosion Inhibition of Lead Objects in Atmospheric Conditions and in Acetic Acid Corrosive Solutions

Elbeshary A. A. Mohammed and Annemie Adriaens * 

Department of Chemistry, Ghent University, Krijgslaan 281 (S12), Ghent 9000, Belgium; elbeshary.ahmed@ugent.be

* Correspondence: annemie.adriaens@ugent.be; Tel.: +32-9264-4826

Received: 8 January 2018; Accepted: 18 March 2018; Published: 23 March 2018



Abstract: In this paper, a saturated long carbon chain sodium monocarboxylate containing 18 carbons—labeled NaC_{18} —was used for the formation of a lead carboxylate coating to inhibit the corrosion of lead in atmospheric conditions and in acetic acid corrosive solutions. The effect of stirring of the coating solution during the coating process on the inhibition efficiency was studied. The coating was characterized by scanning electron microscopy and Fourier transform infrared spectroscopy which have confirmed a formation of lead carboxylate layer on the lead metal surface. The corrosion inhibition properties of the coating were tested using linear sweep voltammetry and electrochemical impedance spectroscopy in a solution simulating the atmospheric conditions and in an acetic acid corrosive solution. Results show that the lead carboxylate forms a protective barrier that inhibits corrosion of lead in atmospheric conditions and in acetic acid corrosive solutions.

Keywords: lead; coating; lead preservation; corrosion; lead carboxylate

1. Introduction

Lead metal has been used in many applications in ancient times because of its high density and ease of casting due to its low melting point. Some of these applications are for water piping, statues, roofing, weights, coins, and pipe organs [1–4]. Many of those objects are exposed to atmospheric conditions and are shown in open museum showcases, where it is difficult to be in full control of the environment. Therefore, they corrode and are naturally covered by corrosion products [5]. The most common corrosion products found on lead metal surfaces are litharge (PbO), anglesite (PbSO_4), and hydroxycarbonate compounds—such as cerussite (PbCO_3), hydrocerussite ($\text{Pb}_3(\text{CO}_3)_2(\text{OH})_2$), or plumbonacrite ($\text{Pb}_{10}(\text{CO}_3)_6\text{O}(\text{OH})_6$) [5,6]. However, those corrosion products do not cover the surface sufficiently to protect the lead metal [5,7,8]. Furthermore, hydrolysis of the wood of the display cases, for instance, releases organic acids. These organic acids, particularly acetic acid, result in an active corrosion which can lead to the loss of these objects [9,10]. Similarly, the lead metal parts of the pipe organs, an important part of the cultural heritage of Europe, corrode by the organic acids which are emitted from the oak wooden wind chest, resulting in the degradation of the pipe structure through pitting and cracking [11,12]. The mechanism of the effect of the acetic acid vapor on the lead metal corrosion is shown in Figure 1.

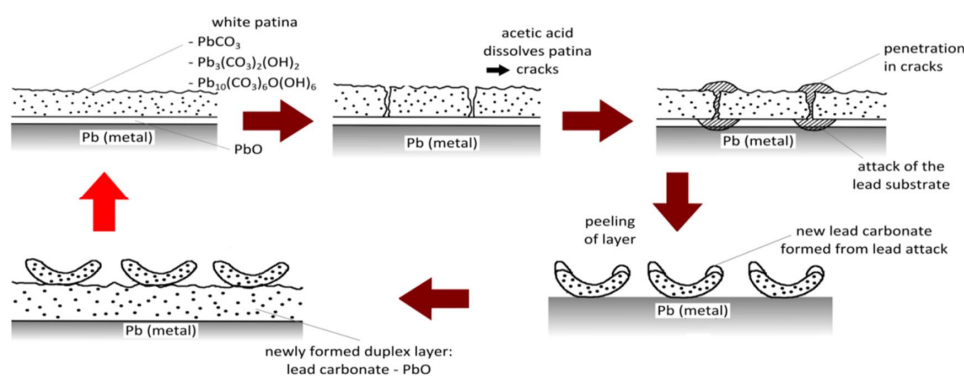


Figure 1. Schematic mechanism of lead corrosion by acetic acid. Reproduced from [13] with permission; Copyright Elsevier 2004.

The organic acids are condensed in aqueous surface film, and the atmospheric corrosion products undergo an acid dissolution to form soluble lead acetates compounds. Then, the concentrated solution of the acetate compounds penetrates the gaps of the corrosion layer towards the lead metal surface leading to the dissolution of the PbO underlayer, followed by the peeling of the carbonates layer. The lead metal then corrodes, forming a new PbO and carbonates layers again. After that, a cyclic corrosion occurs leading to the degradation of the object [5,13]. One way to prevent or delay the corrosion is to use protective coatings. However, the coatings used for protecting cultural heritage objects should be transparent, reversible, stable for long time and environmental friendly. Prior studies have proven that environmentally friendly sodium carboxylates of the chemical formula $\text{CH}_3(\text{CH}_2)_{n-2}\text{COONa}$ ($7 \leq n \leq 12$), denoted as NaC_n , provide preservative coatings for the archaeological lead metal objects [13–19]. Those studies have tried carbon chain lengths up to 12, as those sodium carboxylates with carbon chains more than 12 have low solubility in water. In our previous work [20], we tried longer carbon chain, NaC_{14} and NaC_{18} , in water/ethanol 1:1 (*v/v*) mixture at 50 °C. The coating solution has been kept gently stirred during the immersion to ensure the non-deposition of the solution. The results have revealed the formation of hydrophobic $\text{Pb}(\text{C}_{14})_2$ and $\text{Pb}(\text{C}_{18})_2$ complexes on the lead metal surface, respectively, which act as good barriers protecting it against corrosion in atmospheric conditions. $\text{Pb}(\text{C}_{18})_2$, as it has longer carbon chain, exhibited a better protection than $\text{Pb}(\text{C}_{14})_2$.

In this study, we follow the previous study and work further on the $\text{Pb}(\text{C}_{18})_2$ coating because it revealed better results [20]. In this work, the coating process was done without stirring the coating solution during the immersion as the stirring might lead to remove a part of the coating from the lead metal surface. The formed coating was characterized by Fourier transform infrared spectroscopy (FTIR) and scanning electron microscopy (SEM). The corrosion inhibition efficiency of the formed coating, without stirring, was compared with that of the coating which was formed with stirring. That comparison was done by linear sweep voltammetry (LSV) in a corrosive solution mimicking atmospheric conditions. Furthermore, the protective properties of the coating were examined by linear sweep voltammetry (LSV) and electrochemical impedance spectroscopy (EIS) in an acetic acid corrosive solution.

2. Experimental

2.1. Chemicals

Sodium octadecanoate NaC_{18} was obtained by the neutralization of octadecanoic acid $\text{CH}_3(\text{CH}_2)_{16}\text{COOH}$ (assay $\geq 97\%$, Fluka, Steinheim, Germany). The latter was done by the addition of 50 mL of 1 M NaOH and 50 mL of absolute ethanol to 10 g of the acid. The mixture was stirred while heating to ≤ 90 °C for 30 min in a water bath. Following this procedure, it was cooled in air to the ambient temperature. After the solution had been cooled down, NaC_{18} solidified directly. The product

was filtered off and washed four or five times with water to eliminate the surplus of NaOH. Then, it was then dried in air overnight. The ASTM D1384-87 [21,22] solution (pH = 8.3), denoted in what follows as the ASTM solution, simulates the corrosive atmospheric conditions. The ASTM solution consists of 1.04 mM Na₂SO₄ (Merck, Hohenbrunn, Germany), 1.64 mM NaHCO₃ (Merck, Darmstadt, Germany) and 2.82 mM NaCl (Prolabo, Leuven, Belgium).

The acetic acid corrosive solution (pH = 3.5) is a 0.1 M tetrabutylammonium bromide (TBAB) (purity > 99%, Merck, Darmstadt, Germany) containing 5 µg·L⁻¹ acetic acid (98–99%, Vel NV, Leuven, Belgium). This concentration of the acetic acid is higher than that it was recorded in the wooden show cases or in the wind chests of the organ pipe [23]. TBAB is not aggressive to lead metal, and it is used as a supporting electrolyte to prevent the migration current and decrease the iR drop of the cell [23,24]. Coupons with dimensions 12.6 mm diameter and 2 mm thickness were made from 99.95% lead sheet (Goodfellow Ltd., Cambridge, UK).

2.2. Preparation of the Lead Coupons

The lead coupons were prepared by grinding their surfaces using a wet grinding disc (BuehlerMet II, Buehler, Lake Bluff, IL, USA) to eliminate the surface defects and to obtain a new surface of the metal. Subsequently, the coupons were polished using a polishing cloth (MicroCloth, Buehler, Lake Bluff, IL, USA) saturated with a 6 µm MetaDi polycrystalline diamond suspension, followed by one saturated with a 1 µm MetaDi polycrystalline diamond suspension. The duration of polishing for each diamond suspension was 20 min. In between, the coupons were rinsed with isopropanol (99.5%, reagent grade, Merck) and they were sonicated in isopropanol for 5 min. After the last step of polishing, they were sonicated in isopropanol three times for 5 min. For every sonication time, fresh isopropanol was used. The polishing with the oil-based diamond was performed using an automatic grinder (Minimet 1000, Buehler, Lake Bluff, IL, USA).

2.3. Coating Process

The coating solution (50 mM) was prepared by adding 0.7670 g of NaC₁₈ to a 50 mL of water/ethanol 1:1 (v/v) mixture while stirring at a temperature of 50 °C till the compound dissolved completely.

The polished coupons were exposed to the ambient air for 1 h forming a layer of lead oxide, prior the immersion in the coating solution for 24 h. The solution was kept at 50 °C during immersion, however, no stirring was applied. During the immersion, the sodium carboxylate reacts with the formed lead oxide layer forming lead carboxylate. After the immersion, the coupons were removed and rinsed with a water/ethanol mixture to remove the coating solution suspended with the coupons. Then the coupons were dried overnight in air.

2.4. SEM Experiments

The lead coated coupons were coated by sputtering a carbon on them using a Balzers Union (Balzers, Liechtenstein sputter coater before imaging them with the scanning electron microscope (Phenom-FEI, PhenomWorld, Eindhoven, The Netherlands). The images of the backscattered electrons were registered using a 5 kV electron beam and a four-quadrant solid-state detector.

2.5. Coating Thickness Measurements

The coating thickness was measured with a coating thickness gauge (Check-Line 3000PRO, model DCFN-3000PRO, Bad Bentheim, Germany), which was calibrated using an uncoated sample.

2.6. FTIR Measurements

FTIR spectra were measured in the range from 4400 to 600 nm with a FTIR spectrometer (Spectrum 1000, Perkin-Elmer, Waltham, MA, USA), provided with a horizontal attenuated total

reflection cell (Pike MIRacle, PIKE Technologies, Madison, WI, USA). The collection of spectra was done on two different coated samples at five individual sites on each coated sample.

2.7. LSV Measurements

Potentiodynamic polarization (PDP) was carried out using an Autolab potentiostat (PG-STAT 20, Metrohm, Herisau, Switzerland). The measurements were carried out in an electrochemical cell containing three electrodes. A graphite rod and an Ag/AgCl were used as a counter and a reference electrode, respectively. The PDP plots were recorded in an aerated ASTM solution, and in an aerated 0.1 M TBAB solution containing $5 \mu\text{g}\cdot\text{L}^{-1}$ acetic acid at 25°C in a potential range from -0.8 to $+0.5$ V vs. Ag/AgCl at a scan rate of 3 mV/s .

2.8. EIS Measurements

EIS measurements were carried out using a potentiostat with a frequency response analysis module (FRA module, EcoChemie BV, Utrecht, The Netherlands). The counter and the reference electrodes were, respectively a graphite rod and an Ag/AgCl. The open circuit potential (OCP) took 20 min to measure. Impedance spectra were measured in an aerated 0.1 M TBAB solution containing $5 \mu\text{g}\cdot\text{L}^{-1}$ acetic acid at 25°C at the OCP. The frequency range was 100 kHz to 0.01 Hz, and it was logarithmically distributed upon 120 points. The amplitude was 10 mV.

3. Results and Discussion

3.1. Surface Analysis

3.1.1. SEM Analysis and Coating Thickness Measurements

Figure 2 shows the backscattered electron images of the coating obtained from NaC_{18} without stirring (left side) and NaC_{18} with stirring of the coating solution during the immersion (right side). The micrograph of the coating obtained without stirring is very similar to that of the coating obtained with stirring. In both coatings, lead surfaces seem be covered preferential oriented layers of stacked chip-like crystals. The coating thickness measurements show that the coating thickness obtained in the stirred and the non-stirred procedures was $13 \pm 3 \mu\text{m}$ and $16 \pm 2 \mu\text{m}$, respectively. This indicates that the non-stirred procedure produces a slightly thicker coating in comparison to the stirred procedure. This is because the stirring may lead to removing a part of the coating from the lead metal surface.

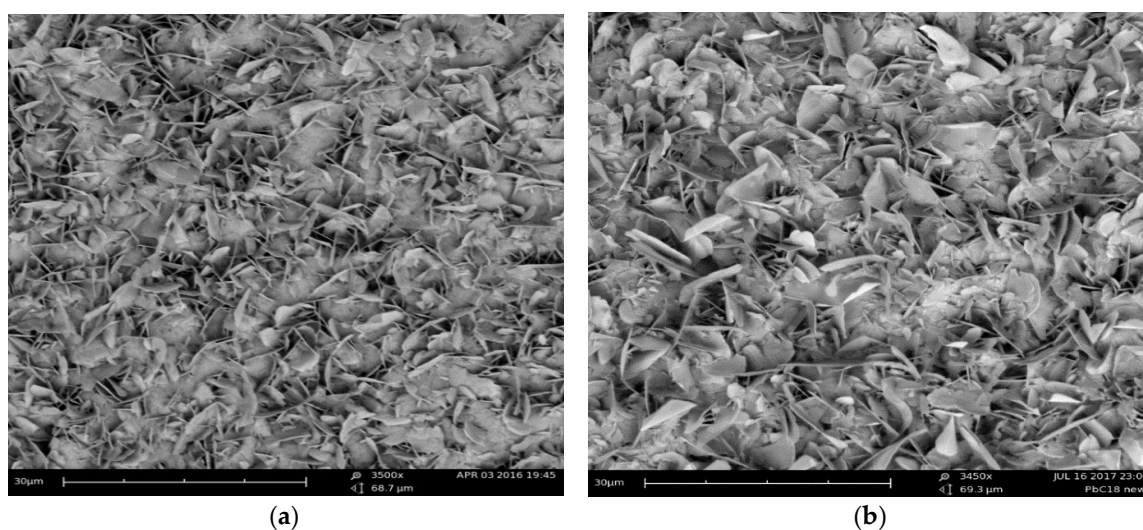


Figure 2. Backscattered electron images of the coating obtained from NaC_{18} without stirring (a) and NaC_{18} with stirring (b).

3.1.2. FTIR Measurements

The coating obtained without stirring was identified by comparing its FTIR spectra with that of the $\text{Pb}(\text{C}_{18})_2$ reference powder [25]. Figure 3 exhibits the FTIR spectra of the coating obtained without stirring (red line) in comparison to that of the $\text{Pb}(\text{C}_{18})_2$ reference powder (black line). The spectrum of the coating is quite similar to that of the reference powder, which confirms the formation of a lead carboxylate coating. In both spectra (the coating and the reference), the absorption bands at 1510 , 1415 , and 696 cm^{-1} are characterized as the antisymmetric mode ν_{as} , symmetric stretching mode ν_{s} , and scissoring bending mode δ_{s} of the carboxylate group, respectively. Both ν_{as} and ν_{s} absorption peaks look like doublets refer to divalent metal carboxylates [26]. Several CH_2 wagging progression absorption peaks are noticed as a group of orderly separated bands from 1345 to 1180 cm^{-1} . These absorption peaks characterize chains in the all-*trans* conformation, and their number are related on the number of the carbons in the aliphatic long carbon carboxylates [27,28]. If N is the number of bands in the 1345 to 1180 cm^{-1} region, then the number of carbons is $2N$ [28]. In our case, the number of bands in the 1345 to 1180 cm^{-1} region is 9. Therefore, the number of carbons is 18 confirming the formation of C_{18} carboxylate. The absorption peaks around 2900 cm^{-1} represent the four symmetric/asymmetric stretching peaks for C–H. Two of these peaks are related to the $-\text{CH}_2-$ and the others are related to the $-\text{CH}_3$ in the carbon chain [25].

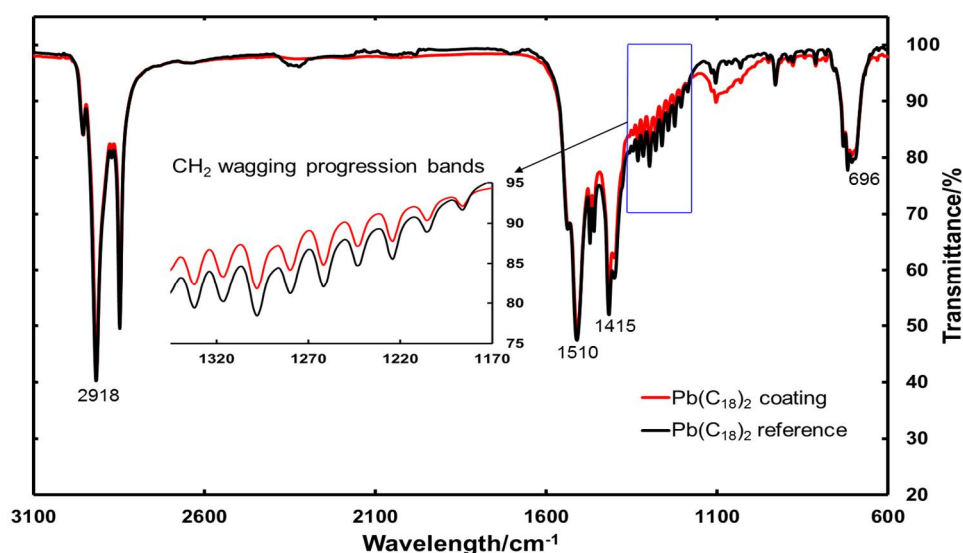


Figure 3. FTIR spectrum of the lead coupon immersed in a 50 mM NaC_{18} in water/ethanol mixture ($\text{Pb}(\text{C}_{18})_2$ coating) and the synthesized $\text{Pb}(\text{C}_{18})_2$ reference complex.

3.2. Electrochemical Measurements

3.2.1. In Atmospheric Conditions

The effect of the stirring of the coating solution during the immersion on the corrosion inhibition efficiency in atmospheric conditions were studied by LSV. PDP curves (Figure 4) of the lead coupons immersed in NaC_{18} with and without stirring, in comparison to an uncoated one, were recorded in an ASTM solution.

Figure 4 demonstrates that both coatings (with and without stirring) reveal significantly low anodic and cathodic current densities in comparison to the uncoated one. The decrease in cathodic and anodic currents densities is noticed for the entire recorded potential range. This proves that the coatings protect the lead sample not only at the corrosion potential E_{corr} , but for the entire potential window. Furthermore, both coated samples show more positive corrosion potentials with regard to the uncoated one. These effects elucidate that both coatings act as good barriers and thereby prevent or

decrease the approach of the corrosive solution to the surface of lead metal. Therefore, they decrease the available active sites for the cathodic (oxygen reduction) and anodic (metal dissolution) corrosion reactions, decelerating the corrosion action [15]. Comparison of the PDP curves obtained from both coatings displays that the coating without stirring shows lower anodic and cathodic currents densities than the coating with stirring. However, the corrosion potential for the coating with stirring is shifted towards the positive direction more than the coating without stirring. From those observations, it can be concluded that the coating without stirring can demonstrate a good equilibrium between the effectiveness and the application easiness.

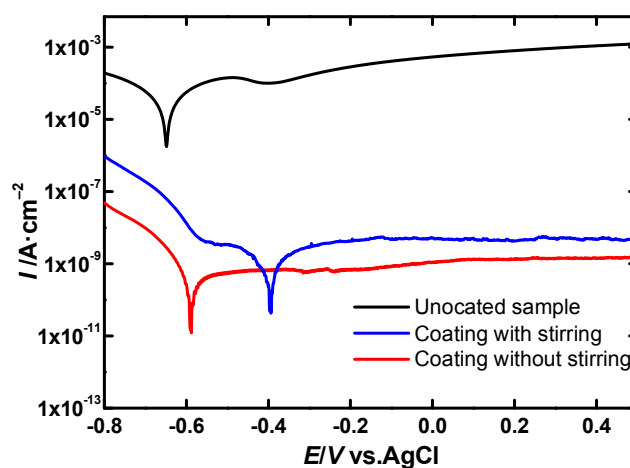


Figure 4. PDP curves in ASTM solution at a scan rate of $3 \text{ mV}\cdot\text{s}^{-1}$ of lead coupons which were immersed in a 50 mM NaCl solution for 24 h.

3.2.2. In an Acetic Acid Corrosive Solution

Based on the above-mentioned results which reveal that the coating obtained without stirring of the coating solution has good protective properties in the atmospheric conditions, the $\text{Pb}(\text{C}_{18})_2$ coating was tested as inhibitor for the corrosion of lead in an acetic acid corrosive solution.

LSV Experiments

Figure 5 shows the potentiodynamic polarization plots which were recorded in the acetic acid corrosive solution by LSV for a lead sample treated in 50 mM NaCl , without stirring, compared to an uncoated sample. Results show that the polarization curves do not exhibit long linear regions at high overpotentials to extrapolate Tafel regions accurately to obtain the intersection points. This can be attributed to that in aerated acid solution, as in our state, the cathodic part of the corrosion reactions is the reduction of the oxygen as represented in the equation [29]:



Therefore, the cathodic limiting current originates from the oxygen diffusion, not from the charge transfer reaction, leading to non-linearity in the Tafel plot [30]. However, the anodic current density for the coated lead sample decreases one order of magnitude with respect to the uncoated one. This can be explained by the fact that the coating has an anodic effect on the corrosion mechanism, where it reduces or retards the dissolution/oxidation of the lead metal, and, consequently, reduces the corrosion of the lead metal. Furthermore, the corrosion potential of the coated sample has shifted to a higher potential in comparison to the uncoated one. This means that the coating forms as a good barrier blocking the anodic area on the lead metal surface [19]. It can also be observed that the coating reveals as a passivation peak. That peak may represent a dissolution of PbO in the pores of the coating or an oxidation of unreacted sodium carboxylate. A comparison of the PDP result of the coating in

acetic acid solution to that in ASTM solution revealed that the coating shows protective properties in the acetic acid solution lower than that in ASTM solution. This is consistent with the work in the literature [9,10,19] which proclaims that the acetic acid accelerates the corrosion of the lead through the dissolution of the lead oxide on the lead metal surface. Therefore, in our case, the acetic acid might dissolve the PbO formed in the pores of the coating leading to an increased corrosion of lead. Hence the lower protective properties of the coating in acetic acid compared to that in the ASTM solution.

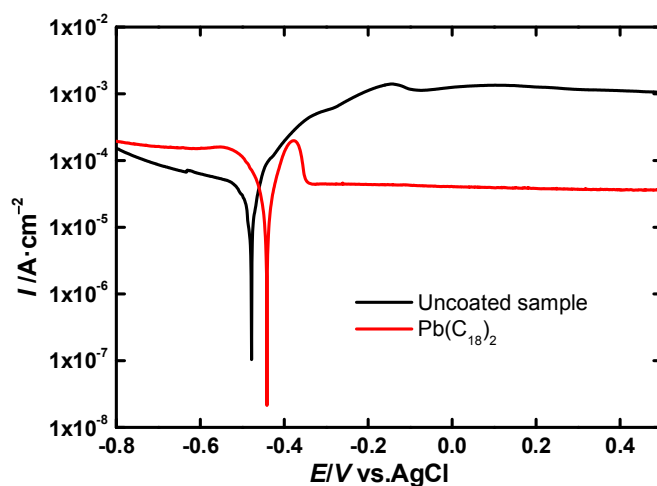


Figure 5. Potentiodynamic curves in a 0.1 M TBAB solution containing $5 \mu\text{g}\cdot\text{L}^{-1}$ acetic acid at a scan rate $3 \text{ mV}\cdot\text{s}^{-1}$ of lead samples coated in a 50 mM NaC_{18} solution for 24 h.

EIS Experiments

Evaluation of the protection efficiency of the $\text{Pb}(\text{C}_{18})_2$ coating in acetic acid solution has been done by EIS measurements. Figure 6 shows the Bode plots of the uncoated and coated lead metal coupons. The plots of the impedance in Figure 6a show that the impedance value, at low frequencies, for the coated sample is about one order higher than that for the uncoated one. This higher magnitude of the impedance reveals that the coating acts as a good barrier preventing the arrival of the corrosive ions to the surface of the lead metal [31]. In Figure 6b, the phase angle plots of the bare coupon display four loops or time constants. Two loops are in the higher frequencies. The first one is an inductive loop, around 100 kHz, which could be arise from an adsorption/desorption process of electrolyte ions on the electrode surface [32]. The second one, around 6.5 kHz, refers to the SiC particle resistance and its dielectric effect. A rational interpretation for the source of those SiC particles is the polishing of the coupons by SiC sheets. Because of the softness of the lead metal, the SiC particles adhere to the lead metal surface and could illustrate the capacitive loop at the high frequencies [19,20]. The third and fourth time constants are in the low frequency range. The third one, at ~ 3.5 Hz is attributed to the resistance of the lead oxide, PbO, layer on the lead metal surface. The fourth one, around 0.03 Hz, is attributed to the electrochemical double layer at the interface of the metal/oxide layer. On the other side, the plot of the phase angle of the coated sample shows two loops in the mid- (at ~ 1 kHz) and the low (around 1 Hz) frequencies range, which refer to the coating resistance, and the electrochemical double layer at the metal/coating interface, respectively. It can be also noticed that the coated sample exhibits a higher phase angle value compared to the uncoated sample, reflecting the protective properties of the coating [33].

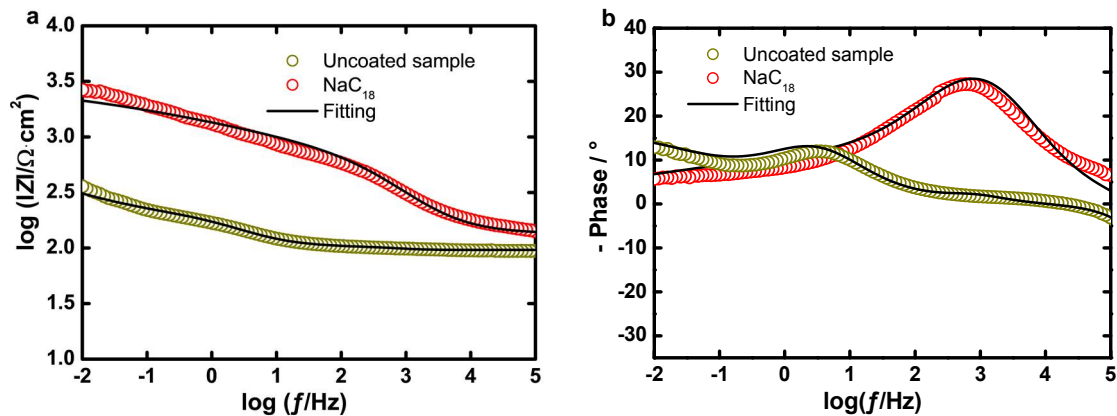


Figure 6. Bode plot in a 0.1 M TBAB solution containing $5 \mu\text{g}\cdot\text{L}^{-1}$ acetic acid of lead coupons coated in a 50 mM NaC_{18} solution for 24 h: (a) modulus plot; (b) phase angle.

A quantitative interpretation of the EIS results of the uncoated and coated samples was carried out by numerical fitting of the experimental data to the equivalent circuits in Figure 6. The Zview software (Version 2.1c), which was developed by McDonald [34], was used for doing the fitting. For the circuit representing the uncoated sample (Figure 7a), L is interpreted as an inductor. The impedance of the inductor can be calculated as described elsewhere [35]. R_U represents the electrolyte resistance. C_{part} and R_{part} refer to the capacitance for the dielectric contribution and the resistance of the SiC particles, respectively. $\text{CPE}_{\text{oxide}}$ and R_{oxide} are a constant phase element related to the capacitance of the oxide layer, and the resistance related to that oxide layer, respectively. CPE_{DL} and R_{CT} represent, respectively, a constant phase element related the electrochemical double layer capacitance and the charge transfer resistance at the interface between the metal and the oxide layer. A constant phase element CPE was used in place of the pure capacitance due to the heterogeneousness of the lead coupon surface and the non-ideal coating capacitance. The capacitance true value of the CPE can be obtained from its specific parameters, as demonstrated in other works [36–38]. The impedance of the CPE, Z_{CPE} , can be obtained by [37,39]

$$Z_{\text{CPE}} = [Y_0(j\omega)^n]^{-1} \quad (2)$$

where Y_0 is the CPE constant, n is the CPE exponent which refers to the heterogeneity ($-1 \leq n \leq 1$), $j = (-1)^{1/2}$, and $\omega = 2\pi f$, where f is the frequency per hertz. When $n = 0$, the CPE is equal to a resistor; when $n = 0.5$, it is equal to a Warburg impedance; when $n = 1$, it is equal to a capacitor; and when $n = -1$, it is equal to an inductor. In the circuit representing the coated sample (Figure 7b), R_U is interpreted as the electrolyte resistance.

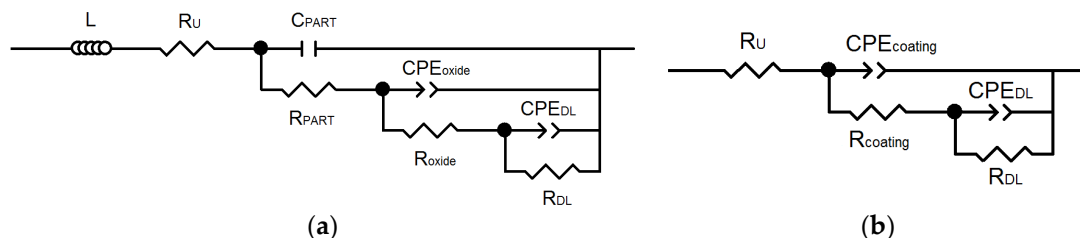


Figure 7. Equivalent circuits used for the numerical fitting of the EIS data for the uncoated (a) and coated (b) samples during immersion in a 0.1 M TBAB solution containing $5 \mu\text{g}\cdot\text{L}^{-1}$ acetic acid.

$\text{CPE}_{\text{coating}}$ and R_{coating} represent a CPE related to the capacitance, and the pores resistance of the coating, respectively. CPE_{DL} and R_{CT} represent a CPE related the electrochemical double layer

capacitance and the charge transfer resistance at the interface between the metal and the oxide layer, respectively. The important parameters of the equivalent circuits which were used for fitting the EIS data are shown in Table 1, together with the goodness of the fitting (χ^2) and the inhibition efficiency percentage (IE %) of the coating. The inhibition efficiency of the coating was calculated from the experimental impedance measurements with the equation [22,39,40]

$$IE(\%) = \frac{R_{CT} - R_{CT}^{\circ}}{R_{CT}} \times 100 \quad (3)$$

where R_{CT} and R_{CT}° are the charge transfer resistances in the presence and absence of the coating, respectively.

Data in the table show that the coating has lower capacitance and a higher pore resistance compared to the bare sample. Therefore, it can be concluded that both coatings act as a hydrophobic barrier [20] hindering the corrosive solution to access the surface of the lead metal, and hence, preventing the corrosion of lead metal. Furthermore, the coating has higher R_{CT} value in comparison to the bare sample. This could be ascribed to the fact that the surface is almost protected by the coating [22]. Finally, it is observed that the values of n_{DL} are 0.45 and 0.25 for the uncoated and coated sample, respectively. This indicates that CPE_{DL} is equivalent to a semi-infinite diffusion rather than to pure capacitors. Hence, this probably points to the ongoing corrosion reactions that have been limited by a diffusion of oxygen and electrolyte towards the electrode, and the Pb^{2+} ions from the electrode surface towards the electrolyte. That diffusion occurs through the PbO layer in case of the uncoated sample or through coating pores in the coated samples [19].

Table 1. The important EIS fitting parameters in a 0.1 M TBAB solution containing $5 \mu\text{g}\cdot\text{L}^{-1}$ acetic acid of lead coupons immersed in 50 mM NaC_{18} solution for 24 h.

Sample	R_U ($\Omega\cdot\text{cm}^2$)	$CPE_{\text{oxide}} - Y_0$ ($\Omega^{-1}\cdot\text{cm}^{-2}\cdot\text{s}^n$)	n_{oxide}	$CPE_{\text{coating}} - Y_0$ ($\Omega^{-1}\cdot\text{cm}^{-2}\cdot\text{s}^n$)	n_{coating}	R_{oxide} ($\Omega\cdot\text{cm}^2$)
Uncoated	96.00	1.69×10^{-3}	0.70	–	–	98.20
$\text{Pb}(\text{C}_{18})_2$	130.50	–	–	8.53×10^{-6}	0.70	–
Sample	R_{coating} ($\Omega\cdot\text{cm}^2$)	$CPE_{DL} - Y_0$ ($\Omega^{-1}\cdot\text{cm}^{-2}\cdot\text{s}^n$)	n_{DL}	R_{CT} ($\Omega\cdot\text{cm}^2$)	IE (%)	χ^2
Uncoated	–	22.00×10^{-3}	0.45	6.00×10^2	–	9.00×10^{-3}
$\text{Pb}(\text{C}_{18})_2$	400.00	5.14×10^{-4}	0.25	2.74×10^3	78.10	28.82×10^{-3}

Long Term Evaluation of the Coating

Long term evaluation of the coatings was achieved by keeping them in the acetic acid solution for 120 h. EIS measurements were done at separate intervals. Figure 8 shows the bode plots for the coating during the durability test. Figure 8a shows that the impedance magnitude at low frequency does not show a significant change during the first immersion hours remaining around the impedance magnitude for the zero time immersion. This indicates that the coating prevents the corrosive solution from reaching the lead metal surface. Later on, the impedance magnitude decreases gradually. This decrease can be attributed to the electrolyte diffusion developing conducting paths inside the coating. After 24 h of immersion, the impedance shows a little increase before reaching some constancy after 96 h immersion. This recovery can be due to the precipitation of insoluble corrosion products blocking those conducting paths in the coatings [41]. For the phase angle plots (Figure 8b), it can be observed that coating, after 120 h immersion, still has two constant times at the mid- and low frequencies as mentioned above. However, some changes occurred. During the first 4 h of immersion, the phase angle related to the coating shows a significant increase, followed by a decrease before reaching some constancy after 96 h immersion. It can be also noticed that the phase angle was shifted towards to lower frequencies. The increase in the phase angle and the shift could be attributed to water uptake through bores/defects present in the coating film [42]. The sequential decrease of the phase

angle can be related to a precipitation of insoluble corrosion products which block the pores/defects leading to a recovery of the coating barrier properties. Finally, it can be seen that the constant time at the frequency around 1 Hz related to the electrochemical double layer at the metal/coating interface did not exhibit a significant change at the first 4 h. With longer immersion times, the behavior of the electrochemical double layer changed from the diffusion to the capacitance which was translated into the increase of the phase angle. This is probably due to the corrosion that occurs as a result from the arrival the corrosive solution to the lead metal surface. After 96 h, the phase angle shows a stability which can be attributed to the insoluble corrosion products that might hinder the electrolyte to pass to the lead metal surface [43].

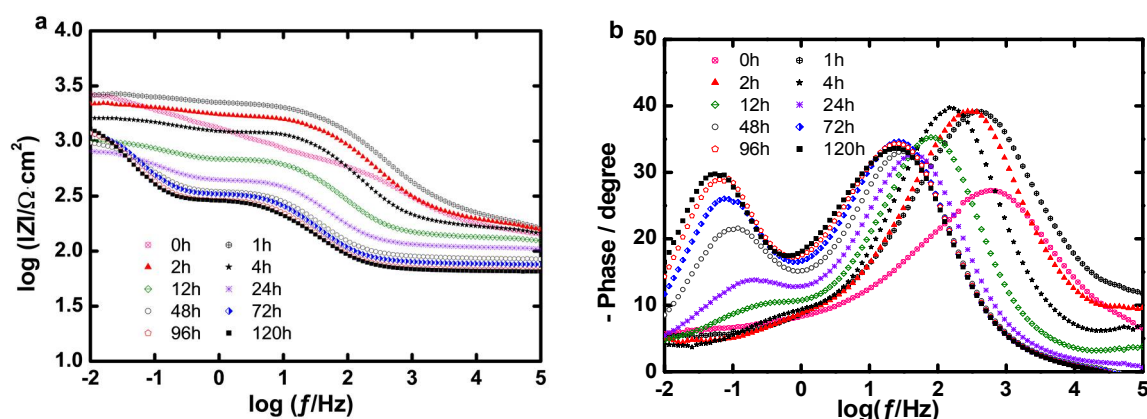


Figure 8. Time evolution of EIS Bode modulus (a) and phase angle (b) plots for lead coupons coated in a 50 mM NaC₁₈ solution for 24 h during immersion in a 0.1 M TBAB solution containing 5 µg·L⁻¹.

4. Conclusions

This work demonstrates the formation of a Pb(C₁₈)₂ coating on a lead metal surface. The coating was obtained by immersing a lead object in a 50 mM NaC₁₈ 1:1 (*v/v*) water/ethanol mixture. The coating was characterized by SEM and FTIR which have shown that the coating appears as preferential oriented layers of chip-like crystals with a chemical structure as a long-chain bivalent metal carboxylate. The effect of the stirring of the coating solution on the coating inhibition in atmospheric condition (ASTM solution) was studied by LSV which showed that the coating without stirring could demonstrate a good equilibrium between the effectiveness and the application ease. The protective properties of the coating without stirring was examined in an acetic acid solution by LSV and EIS. The coating demonstrated good protective properties against lead corrosion, where it exhibited a decrease in corrosion current density, an increase in the corrosion potential and an increase in the charge transfer resistance compared to the uncoated sample. The durability of the coating without stirring was evaluated with the use of EIS which showed that the coating stays on the surface for 120 h. The electrolyte reached the lead metal surface through the pores of the coating, leading to corrosion. However, the formation of insoluble corrosion products led to a recovery of the coating barrier properties.

Acknowledgments: The authors thank Rosie Grayburn for providing the FTIR data of the synthesized Pb(C₁₈)₂ reference material.

Author Contributions: Elbeshary A. A. Mohammed conceived and designed the experiments, performed the experiments, analyzed the data, and wrote the manuscript; Annemie Adriaens contributed the critical revisions.

Conflicts of Interest: The authors declare no conflict of interest.

References

1. Tylecote, R.F. The behaviour of lead as a corrosion resistant medium undersea and in soils. *J. Archaeol. Sci.* **1983**, *10*, 397–409. [[CrossRef](#)]
2. Chiavari, C.; Martini, C.; Prandstraller, D.; Niklasson, A.; Johansson, L.G.; Svensson, J.E.; Åslund, A.; Bergsten, C.J. Atmospheric corrosion of historical organ pipes: The influence of environment and materials. *Corros. Sci.* **2008**, *50*, 2444–2455. [[CrossRef](#)]
3. Donais, M.K.; Whissel, G.; Dumas, A.; Golden, K. Analyzing lead content in ancient bronze coins by flame atomic absorption spectroscopy. An archaeometry laboratory with nonscience majors. *J. Chem. Educ.* **2009**, *86*, 343–346. [[CrossRef](#)]
4. Abu-baker, A.; Sekhaneh, W.A.; Shiyab, A.; Dellith, J.; Scheffel, A.; Alebrahim, M.A. Analytical investigation of five roman Pb-based scale weights (Qasr Ar-Rabbah, Jordan): A Case Study. *Mediterr. Archaeol. Archaeom.* **2014**, *14*, 181–190.
5. Graedel, T. Chemical mechanisms for the atmospheric corrosion of lead. *J. Electrochem. Soc.* **1994**, *141*, 922–927. [[CrossRef](#)]
6. Tranter, G.C. Patination of lead: An infra-red spectroscopic study. *Br. Corros. J.* **1976**, *11*, 222–224. [[CrossRef](#)]
7. Watkinson, D. Preservation of metallic cultural heritage. In *Shreir's Corrosion*; Cottis, B., Graham, M., Lindsay, R., Lyon, S., Richardson, T., Scantlebury, D., Stott, H., Eds.; Elsevier Ltd.: Amsterdam, The Netherlands, 2010.
8. Grayburn, R.; Dowsett, M.; De Keersmaecker, M.; Westenbrink, E.; Covington, J.A.; Crawford, J.B.; Hand, M.; Walker, D.; Thomas, P.A.; Banerjee, D.; et al. Time-lapse synchrotron X-ray diffraction to monitor conservation coatings for heritage lead in atmospheres polluted with oak-emitted volatile organic compounds. *Corros. Sci.* **2014**, *82*, 280–289. [[CrossRef](#)]
9. Niklasson, A.; Johansson, L.-G.; Svensson, J.-E. The influence of relative humidity and temperature on the acetic acid vapour-induced atmospheric corrosion of lead. *Corros. Sci.* **2008**, *50*, 3031–3037. [[CrossRef](#)]
10. Niklasson, A.; Johansson, L.-G.; Svensson, J.-E. Influence of acetic acid vapor on the atmospheric corrosion of lead. *J. Electrochem. Soc.* **2005**, *152*, B519–B525. [[CrossRef](#)]
11. Niklasson, A.; Johansson, L.-G.; Svensson, J.-E. Atmospheric corrosion of historical organ pipes: Influence of acetic and formic acid vapour and water leaching on lead. In *Metal 04: Proceedings of the International Conference on Metals Conservation: Canberra, Australia, 4–8 October 2004*; Ashton, J., Hallam, D., Eds.; National Museum of Australia: Canberra, Australia, 2004; pp. 273–280.
12. Chiavari, C.; Martini, C.; Poli, G.; Prandstraller, D. Conservation of organ pipes: protective treatments of lead exposed to acetic acid vapours. In *Metal 04: Proceedings of the International Conference on Metals Conservation: Canberra, Australia, 4–8 October 2004*; Ashton, J., Hallam, D., Eds.; National Museum of Australia: Canberra, Australia, 2004.
13. Rocca, E.; Rapin, C.; Mirambet, F. Inhibition treatment of the corrosion of lead artefacts in atmospheric conditions and by acetic acid vapour: Use of sodium decanoate. *Corros. Sci.* **2004**, *46*, 653–665. [[CrossRef](#)]
14. Rocca, E.; Steinmetz, J. Inhibition of lead corrosion with saturated linear aliphatic chain monocarboxylates of sodium. *Corros. Sci.* **2001**, *43*, 891–902. [[CrossRef](#)]
15. De Keersmaecker, M.; Verbeken, K.; Adriaens, A. Lead dodecanoate coatings for the protection of lead and lead-tin alloy artifacts: Two examples. *Appl. Surf. Sci.* **2014**, *292*, 149–160. [[CrossRef](#)]
16. Dowsett, M.; Adriaens, A.; Schotte, B.; Jones, G.; Bouchenoire, L. In-situ spectroelectrochemical study of the growth process of a lead decanoate coating as corrosion inhibitor for lead surfaces. *Surf. Interface Anal.* **2009**, *41*, 565–572. [[CrossRef](#)]
17. De Wael, K.; De Keersmaecker, M.; Dowsett, M.; Walker, D.; Thomas, P.A.; Adriaens, A. Electrochemical deposition of dodecanoate on lead in view of an environmentally safe corrosion inhibition. *J. Solid State Electrochem.* **2010**, *14*, 407–413. [[CrossRef](#)]
18. Adriaens, A.; De Bisschop, F.; Dowsett, M.; Schotte, B. Growth and real time corrosion resistance monitoring of lead decanoate coatings. *Appl. Surf. Sci.* **2008**, *254*, 7351–7355. [[CrossRef](#)]
19. De Keersmaecker, M.; Depla, D.; Verbeken, K.; Adriaens, A. Electrochemical and surface study of neutralized dodecanoic acid on a lead substrate. *J. Electrochem. Soc.* **2014**, *161*, C126–C137. [[CrossRef](#)]

20. Mohammed, E.A.A.; De Keersmaecker, M.; Verbeken, K.; Adriaens, A. Saturated long linear aliphatic chain sodium monocarboxylates for the corrosion inhibition of lead objects—An initiative towards the conservation of our lead cultural heritage. *J. Solid State Electrochem.* **2017**, *21*, 693–704. [[CrossRef](#)]
21. Mirambet, F.; Reguer, S.; Rocca, E.; Hollner, S.; Testemale, D. A complementary set of electrochemical and X-ray synchrotron techniques to determine the passivation mechanism of iron treated in a new corrosion inhibitor solution specifically developed for the preservation of metallic artefacts. *Appl. Phys. A Mater. Sci. Process.* **2010**, *99*, 341–349. [[CrossRef](#)]
22. Mohammed, E.A.A.; De Keersmaecker, M.; Adriaens, A. Inhibition of the corrosion of iron heritage objects after treatment with long-chain monocarboxylic acids in ethanolic solutions. *Prog. Org. Coat.* **2016**, *101*, 225–232. [[CrossRef](#)]
23. De Keersmaecker, M.; Berg, O.V.D.; Verbeken, K.; Depla, D.; Adriaens, A. Hydrogenated dimer acid as a corrosion inhibitor for lead metal substrates in acetic acid. *J. Electrochem. Soc.* **2015**, *162*, C167–C179. [[CrossRef](#)]
24. De Keersmaecker, M. The Development of an Environmentally Friendly Coating for the Corrosion Inhibition of Lead Objects. Ph.D. Thesis, Ghent University, Ghent, Belgium, December 2015.
25. Grayburn, R. *Spectroelectrochemical Techniques for the Conservation of Metallic Artefacts*; Ghent University: Ghent, Belgium, 2015.
26. Mesubi, M.A. An infraed study of zinc, cadmiun and lead salts of some fatty acid. *J. Mol. Struct.* **1982**, *81*, 61–71. [[CrossRef](#)]
27. Colthup, N.B.; Daly, L.H.; Wiberley, S.E. *Introduction to Infrared and Raman Spectroscopy*, 2nd ed.; Academic Press: New York, NY, USA, 1975.
28. Lin-Vien, D.; Colthup, N.B.; Fateley, W.G.; Grasselli, J.G. *The Handbook of Infrared and Raman Characteristic Frequencies of Organic Molecules*; Academic Press: San Diego, CA, USA, 1991.
29. Stansbury, E.E.; Buchanan, R.A. *Fundamentals of Electrochemical Corrosion*, 1st ed.; ASM International: Novelty, OH, USA, 2000.
30. Wessel, J.K. *Handbook of Advanced Materials: Enabling New Designs*; Wessel, J.K., Ed.; John Wiley & Sons, Inc.: Hoboken, NJ, USA, 2004.
31. Grandle, J.A.; Taylor, S.R. Electrochemical impedance spectroscopy of coated aluminum beverage containers: Part 1—Determination of an Optimal Parameter for Large Sample Evaluation. *Corrosion* **1994**, *50*, 792–803. [[CrossRef](#)]
32. Valero Vidal, C.; Igual Muñoz, A. Electrochemical aspects in biomedical alloy characterization: Electrochemical impedance spectroscopy. In *Biomedical Engineering, Trends in Materials Science*; Laskovski, A., Ed.; InTech: Rijeka, Croatia, 2011.
33. Loveday, D.; Peterson, P.; Rodgers, B. Evaluation of organic coatings with electrochemical impedance spectroscopy. Part 1: Fundamentals of electrochemical impedance spectroscopy. *J. Coat. Technol.* **2004**, *1*, 46–52.
34. Hassanzadeh, A. Validity of dynamic electrochemical impedance spectra of some amine corrosion inhibitors in petroleum/water corrosive mixtures by Kramers-Kronig transformation. *Corros. Sci.* **2007**, *49*, 1895–1906. [[CrossRef](#)]
35. Pham, K.-C.; McPhail, D.S.; Mattevi, C.; Wee, A.T.S.; Chua, D.H.C. Graphene-carbon nanotube hybrids as robust catalyst supports in proton exchange membrane fuel cells. *J. Electrochem. Soc.* **2016**, *163*, F255–F263. [[CrossRef](#)]
36. Brug, G.J.; van den Eeden, A.L.G.; Sluyters-Rehbach, M.; Sluyters, J.H. The analysis of electrode impedances complicated by the presence of a constant phase element. *J. Electroanal. Chem. Interfacial Electrochem.* **1984**, *176*, 275–295. [[CrossRef](#)]
37. Amirudin, A.; Thierry, D. Application of electrochemical impedance spectroscopy to study the degradation of polymer-coated metals. *Prog. Org. Coat.* **1995**, *26*, 1–28. [[CrossRef](#)]
38. Hirschorn, B.; Orazem, M.E.; Tribollet, B.; Vivier, V.; Frateur, I.; Musiani, M. Determination of effective capacitance and film thickness from constant-phase-element parameters. *Electrochim. Acta* **2010**, *55*, 6218–6227. [[CrossRef](#)]
39. Cano, E.; Lafuente, D.; Bastidas, D.M. Use of EIS for the evaluation of the protective properties of coatings for metallic cultural heritage: A review. *J. Solid State Electrochem.* **2010**, *14*, 381–391. [[CrossRef](#)]

40. Oguzie, E.; Wang, S.; Li, Y.; Wang, F. Corrosion and corrosion inhibition characteristics of bulk nanocrystalline ingot iron in sulfuric acid. *J. Solid State Electrochem.* **2008**, *12*, 721–728. [[CrossRef](#)]
41. Behzadnasab, M.; Mirabedini, S.M.; Kabiri, K.; Jamali, S. Corrosion performance of epoxy coatings containing silane treated ZrO₂ nanoparticles on mild steel in 3.5% NaCl solution. *Corros. Sci.* **2011**, *53*, 89–98. [[CrossRef](#)]
42. Suegama, P.H.; Fugivara, C.S.; Benedetti, A.V.; Fernández, J.; Espallargas, N.; Delgado, J.; Guilemany, J.M. Microstructure and electrochemical studies of Cr₃C₂-NiCr coatings obtained by HVOF. In *New Research on Electrochemistry*; Vargus, E.P., Ed.; Nova Science Publishers, Inc.: New York, NY, USA, 2007.
43. Zandi Zand, R.; Flexer, V.; De Keersmaecker, M.; Verbeken, K.; Adriaens, A. Self-healing silane coatings of cerium salt activated nanoparticles. *Mater. Corros.* **2016**, *67*, 693–701. [[CrossRef](#)]



© 2018 by the authors. Licensee MDPI, Basel, Switzerland. This article is an open access article distributed under the terms and conditions of the Creative Commons Attribution (CC BY) license (<http://creativecommons.org/licenses/by/4.0/>).